A dual function of V0-ATPase a1 provides an endolysosomal degradation mechanism in *Drosophila melanogaster* photoreceptors

W. Ryan Williamson,[1] Dong Wang,[1] Adam S. Haberman,[1] and P. Robin Hiesinger[1,2]

[1]Department of Physiology and [2]Green Center for Systems Biology, University of Texas Southwestern Medical Center, Dallas, TX 75390

The vesicular adenosine triphosphatase (v-ATPase) is a proton pump that acidifies intracellular compartments. In addition, mutations in components of the membrane-bound v-ATPase V0 sector cause acidification-independent defects in yeast, worm, fly, zebrafish, and mouse. In this study, we present a dual function for the neuron-specific V0 subunit a1 orthologue *v100* in *Drosophila melanogaster*. A *v100* mutant that selectively disrupts proton translocation rescues a previously characterized synaptic vesicle fusion defect and vesicle fusion with early endosomes. Correspondingly, V100 selectively interacts with syntaxins on the respective target membranes, and neither synaptic vesicles nor early endosomes require *v100* for their acidification. In contrast, V100 is required for acidification once endosomes mature into degradative compartments. As a consequence of the complete loss of this neuronal degradation mechanism, photoreceptors undergo slow neurodegeneration, whereas selective rescue of the acidification-independent function accelerates cell death by increasing accumulations in degradation-incompetent compartments. We propose that V100 exerts a temporally integrated dual function that increases neuronal degradative capacity.

Introduction

Neurons have highly specialized demands on intracellular trafficking during development and function (Sann et al., 2009). Although disruption of endosomal sorting typically leads to early developmental defects, aberrant late endosomal, lysosomal, or autophagic functions have been implicated in neurodegeneration (Mizushima et al., 2008; Nixon et al., 2008; Tooze and Schiavo, 2008). Many disease-causing mutations directly affect degradation pathways, and a common hallmark of neurodegenerative disorders are accumulations of undegraded proteins. Disruption of the autophagy pathway in postdevelopmental neurons in mice leads to neurodegeneration within weeks (Hara et al., 2006; Komatsu et al., 2006). Despite the apparent susceptibility of neurons in particular, the intracellular degradation machinery is thought to be shared with other cell types, and there is little evidence for a dedicated neuronal degradation mechanism.

Most intracellular compartments require acidification to function, and all require targeted membrane fusion to obtain and deliver intracellular cargo. The vesicular ATPase (v-ATPase) is a multisubunit complex that consists of the membrane-bound V0 sector and a cytosolic V1 sector. V0 and V1 assembly is reversible. The V0V1 holoenzyme acidifies intracellular compartments and is required for membrane protein sorting and degradation (Nishi and Forgac, 2002; Marshansky and Futai, 2008). Loss of v-ATPase–dependent acidification leads to signaling defects in early development in *Drosophila melanogaster* (Yan et al., 2009) and *Caenorhabditis elegans* (Kolotuev et al., 2009). In addition, several studies in yeast, worm, fly, zebrafish, and mouse suggest acidification-independent roles for the V0 complex in secretion or membrane fusion. These roles include yeast vacuolar fusion (Peters et al., 2001) and synaptic vesicle exocytosis in *Drosophila* (Hiesinger et al., 2005), Hedgehog secretion in *C. elegans* (Liégeois et al., 2006), insulin secretion (Sun-Wada et al., 2006)

W.R. Williamson and D. Wang contributed equally to this paper.

Correspondence to P. Robin Hiesinger: robin.hiesinger@utsouthwestern.edu

Abbreviations used in this paper: AV, autophagosomal vacuole; Avl, Avalanche; CSP, cystein string protein; ERG, electroretinogram; IP, immunoprecipitation; MARCM, mosaic analysis with a repressible cell marker; MVB, multivesicular body; v-ATPase, vesicular ATPase; WT, wild type.

The Rockefeller University Press $30.00
J. Cell Biol. Vol. 189 No. 5 885–899
www.jcb.org/cgi/doi/10.1083/jcb.201003062

and osteoclast fusion (Lee et al., 2006) in mouse, and phagosome–lysosome fusion in zebrafish (Peri and Nüsslein-Volhard, 2008). The v-ATPase thus represents a molecular machine that may regulate intracellular trafficking by integrating the two basic cellular functions of acidification and membrane fusion (Nishi and Forgac, 2002; Wada et al., 2008). The reversible assembly of the V0 and V1 sectors provides an elegant regulatory mechanism for V0V1 holoenzyme activity. V0V1 disassembly may also regulate the availability of the V0 sector in the membrane for acidification-independent functions (Nishi and Forgac, 2002; Marshansky and Futai, 2008). It is unclear how both functions could be coordinated and integrated to regulate intracellular trafficking.

The *Drosophila* gene *vha100-1* (*v100*) encodes subunit a1 of the V0 sector. Mutations in *v100* were originally identified in a genetic screen for synaptic malfunction (Hiesinger et al., 2005). The genomes of *Drosophila*, *C. elegans*, mouse, and human contain four subunit a1–a4 homologues (Marshansky and Futai, 2008). Mutations in subunit a2 have been shown to cause autosomal recessive cutis laxa type II (wrinkly skin syndrome), and mutations in subunit a3 cause osteopetrosis (Kornak et al., 2000, 2008). *Drosophila* and *C. elegans* subunit a1 orthologues exhibit neuron-specific expression, and a mammalian subunit a1 was originally cloned from a vesicle preparation from bovine brain (Perin et al., 1991). Neuronal expression of *v100* in null mutant embryos is sufficient to rescue embryonic lethality to adulthood in *Drosophila* (Hiesinger et al., 2005). In addition to this cell specificity, subunit a1–a4 homologues confer intracellular compartment specificity. For example, in yeast, there are two subunit "a" homologues, whereas all other 13 core subunits are encoded by a single gene. Of these two, Vph1p localizes to the vacuole, and Stv1p localizes the v-ATPase to the Golgi and endosomal compartments (Manolson et al., 1994; Kane, 2007). A *Torpedo* a1 subunit was shown to be specifically sorted to nerve terminals (Morel et al., 2003). How this compartment-specific targeting of the v-ATPase is mediated by subunit "a" homologues is unknown. An active role of subunit a1–a4 homologues in targeting of vesicle populations or their cargo has, to our knowledge, not been shown.

In this study, we report a dual function of subunit a1 in *Drosophila* that provides an integrated neuronal degradation mechanism. First, V100 directs vesicle fusion independently of acidification. Second, V100 is required for the acidification of a subset of neuronal lysosomes and autophagosomes but not synaptic vesicles and early endosomes. Collectively, these findings show how two completely different molecular functions can be temporally and functionally integrated to provide a cell biological mechanism of "sort and degrade." We propose that V100's dual function provides a neuronal degradation mechanism that functions only after neuronal differentiation in addition to essential endolysosomal function and bestows neurons an increased degradative capacity.

Results

A putative *v100* acidification mutant that rescues neurotransmission

We previously reported synaptic transmission defects in neurons mutant for *v100*, the gene that encodes the v-ATPase V0 subunit a1 in *Drosophila*. Importantly, electrophysiological recordings revealed normal neurotransmitter content of synaptic vesicles in this mutant. Because neurotransmitter loading requires synaptic vesicle acidification, we concluded that V100 is not part of the proton pump that acidifies synaptic vesicles (Hiesinger et al., 2005). These findings not only suggest a second function for *v100* but also raise the question of whether it has a v-ATPase–dependent acidification function elsewhere.

To genetically dissect the two putative functions of V100, we set out to generate a mutation that specifically disrupts the proton translocation function of V100. Such a mutation has been described previously for the yeast orthologue *vph1*; mutation of arginine 735 to alanine (R735A) in *vph1* leads to the specific disruption of proton translocation without affecting assembly of the v-ATPase or its localization (Kawasaki-Nishi et al., 2001). This arginine lies in a 17–amino acid region that is 100% conserved in V100 homologues from yeast to humans and corresponds to R755 in V100 (Fig. 1 A). Neurotransmission in *v100*-null mutant photoreceptors can be rescued using the GAL4/UAS system (Brand and Perrimon, 1993) by exclusively expressing *v100* presynaptically (Hiesinger et al., 2005). We generated and selected two independent UAS-$v100^{R755A}$ lines that exhibit indistinguishable expression levels of the synaptically localized protein compared with control UAS-$v100^{WT}$ (unpublished data). Remarkably, synaptic transmission, as indicated by the on transient of the electroretinogram (ERG), is significantly restored by $v100^{R755A}$ expression in *v100* mutant photoreceptors (Fig. 1, B and C). Surprisingly, however, the rescue of the ERG on transient is accompanied by a significant decrease in ERG depolarization (Fig. 1 D). This reduction in response amplitude does not occur in *v100*-null mutants. Furthermore, the decrease in depolarization is more pronounced when $v100^{R755A}$ is expressed in mutant photoreceptors compared with its overexpression in wild-type (WT) neurons (Fig. 1, B and D). A reduction in response amplitude often indicates an unhealthy neuron. Indeed, even mildly elevated levels of $v100^{R755A}$ in mutant neurons leads to a reduced eye size and loss of photoreceptors (Fig. 1, E–I). In contrast, this phenotype is not observed when $v100^{R755A}$ is expressed at the same level in the presence of WT *v100* (Fig. 1, compare G with I). Higher levels of expression (>24°C) lead to almost complete abolishment of the eye when $v100^{R755A}$ is expressed in *v100*-null mutant photoreceptors and a milder rough eye phenotype when $v100^{R755A}$ or WT *v100* are expressed in WT photoreceptors (unpublished data). Thus, $v100^{R755A}$ has a strongly detrimental effect on photoreceptor viability only when WT *v100* is absent. These observations raise two questions: first, how can expression of $v100^{R755A}$ rescue neurotransmitter release yet cause cell death when expressed at higher levels in mutant neurons? Second, why is $v100^{R755A}$ strongly detrimental to cell viability only in the absence of WT *v100*? $v100^{R755A}$ exhibits a genetically unusual behavior: it is not a dominant negative because it causes a phenotype that is very different from the null mutant and because it does not cause the same phenotype when expressed in a WT background. If $V100^{R755A}$ is selectively disrupted in proton translocation, a straightforward hypothesis would be that $v100^{R755A}$ rescues a second, acidification-independent function that is sufficient to restore neurotransmitter release but

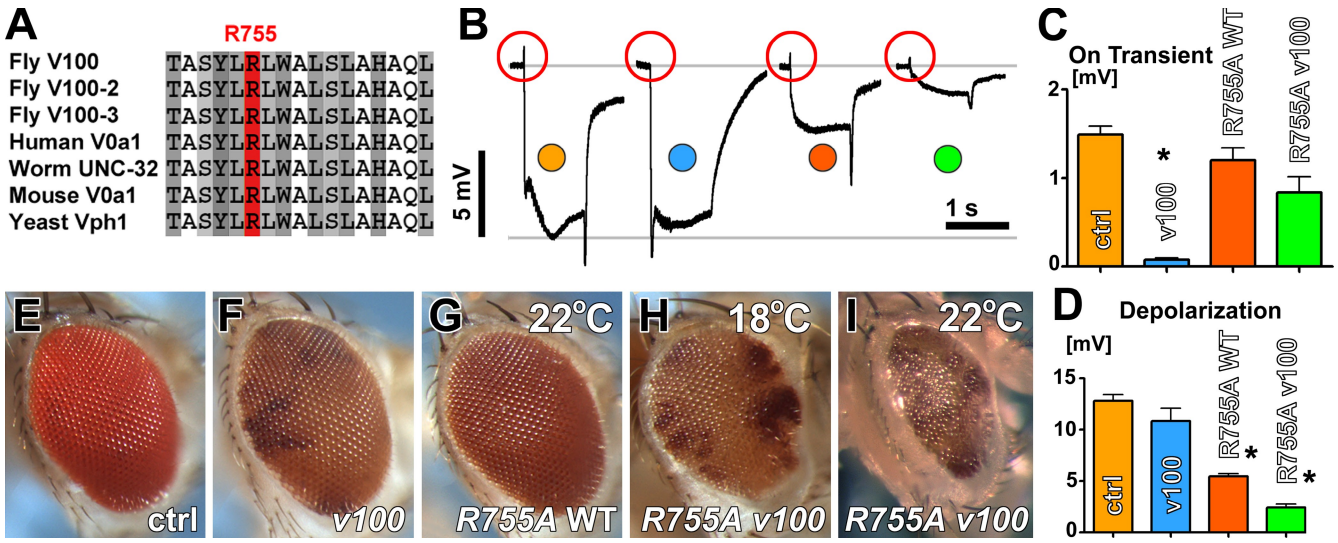

Figure 1. **A *v100* mutant that rescues neurotransmission but causes cell death at high levels.** (A) Alignment of 17 amino acids surrounding the arginine at position 755 (R755) shows 100% conservation across species. (B) Neurotransmitter release rescue experiments. Representative ERG traces from left to right show control (ctrl; yellow), *v100*-null mutant (*ey*FLP eye mosaic; blue), $v100^{R755A}$ expression in WT photoreceptors (red), and $v100^{R755A}$ expression in *v100* mutant photoreceptors (green). Note that rescue with $v100^{R755A}$ exhibits opposite phenotypes from the null mutant: rescue of the on transient (red circles) and a strong reduction of the response amplitude (depolarization). (C) Quantification of on transients for all four genotypes. (D) Quantification of depolarization for all four genotypes. $v100^{R755A}$ in a WT background (red) and $v100^{R755A}$ in a mutant background (green) compared with control (orange) and mutant (blue) are shown. (E–I) Eye pictures show dosage-dependent loss of photoreceptors upon $v100^{R755A}$ expression in the mutant (H and I) but not upon $v100^{R755A}$ expression in WT (G). Error bars indicate SEM. Asterisks denote statistical significance in pairwise comparisons with control ($P < 0.001$).

causes detrimental effects to the cell only in the absence of a WT protein.

V100 is required for the acidification of a subset of neuronal degradative compartments

First, we needed to know whether $v100^{R755A}$ is indeed acidification defective. No acidification role of V100 has so far been characterized (Hiesinger et al., 2005). Therefore, we performed live measurements of intracompartmental pH using the fluorescent probe Lysotracker in the null mutant, $v100^{R755A}$, and control photoreceptors. Lysotracker is a membrane-permeable compound that can be added to the bath of a live *Drosophila* larval or pupal eye–brain culture and selectively labels strongly acidified compartments. To quantitatively assess even slight differences in Lysotracker labeling, we generated 50% fluorescently labeled mutant clones in developing photoreceptor neurons (mosaic analysis with a repressible cell marker [MARCM] technique; Lee and Luo, 1999). As a further control, we confirmed that WT MARCM clones cause no effect (unpublished data). As shown in Fig. 2 A, Lysotracker labeling of mutant and control cells is indistinguishable in L3 larval eye discs, i.e., at the time point when neuronal differentiation and *v100* expression commence. Remarkably, however, in mutant cells at 20% of pupal development (P + 20%), the Lysotracker signal reduces slightly but significantly (unpublished data). At P + 40%, the Lysotracker signal is reduced to ~50% (Fig. 2, B and D). A level of ~50% Lysotracker labeling is maintained in 1-d adult photoreceptors (unpublished data). This phenotype is rescued by expression of WT *v100* (Fig. 2 D). The change of Lysotracker fluorescence is reflected in a corresponding loss of Lysotracker-positive compartments in mutant compared with control clones from 100% in L3 to 67% at P + 20% and 47% at P + 40%. These observations indicate that developing photoreceptors exhibit a progressive reduction of strongly acidified compartments after neuronal differentiation.

Next, we tested whether expression of $v100^{R755A}$ under the same conditions that rescue neurotransmitter release also rescues this acidification defect. As shown in Fig. 2 (C and D), expression of $v100^{R755A}$ in *v100* mutant photoreceptors does not rescue the Lysotracker defect observed in *v100* mutant neurons. This result supports a direct acidification function of V100 for at least some Lysotracker-positive compartments in neurons.

Because Lysotracker labeling indicates normal levels of acidification before neuronal differentiation, we wondered whether these compartments are acidified by other v-ATPase subunits. We tested this idea pharmacologically with the v-ATPase–specific blocker bafilomycin 1A. Indeed, 10-min preincubation with bafilomycin A1 fully prevents any Lysotracker labeling in both mutant and control cells, indicating that these Lysotracker-positive compartments are acidified in a v-ATPase–dependent manner (Fig. 2, F–H). The finding that strongly acidified compartments persist in *v100* mutant neurons shows that *v100* cannot be required equally for the acidification of all compartments.

We assessed the molecular nature of Lysotracker-positive compartments in the live preparation by expressing YFP-tagged versions of the early endosomal maker Rab5, the late endosomal marker Rab7, and the recycling endosomal marker Rab11 (Zhang et al., 2007) as well as the autophagosomal marker Atg8-GFP (Chang and Neufeld, 2009). As shown in Fig. 2 E and Fig. S1 (A and B), Lysotracker rarely marks Rab5- or Rab11-positive compartments. In contrast, 32% of Lysotracker-positive compartments are Rab7-positive, ring-shaped late endosomes. In addition, 20% of Lysotracker-positive compartments are Atg8-GFP positive (Fig. 2 E; and Fig. S1, C and D). This ratio of Rab7- and

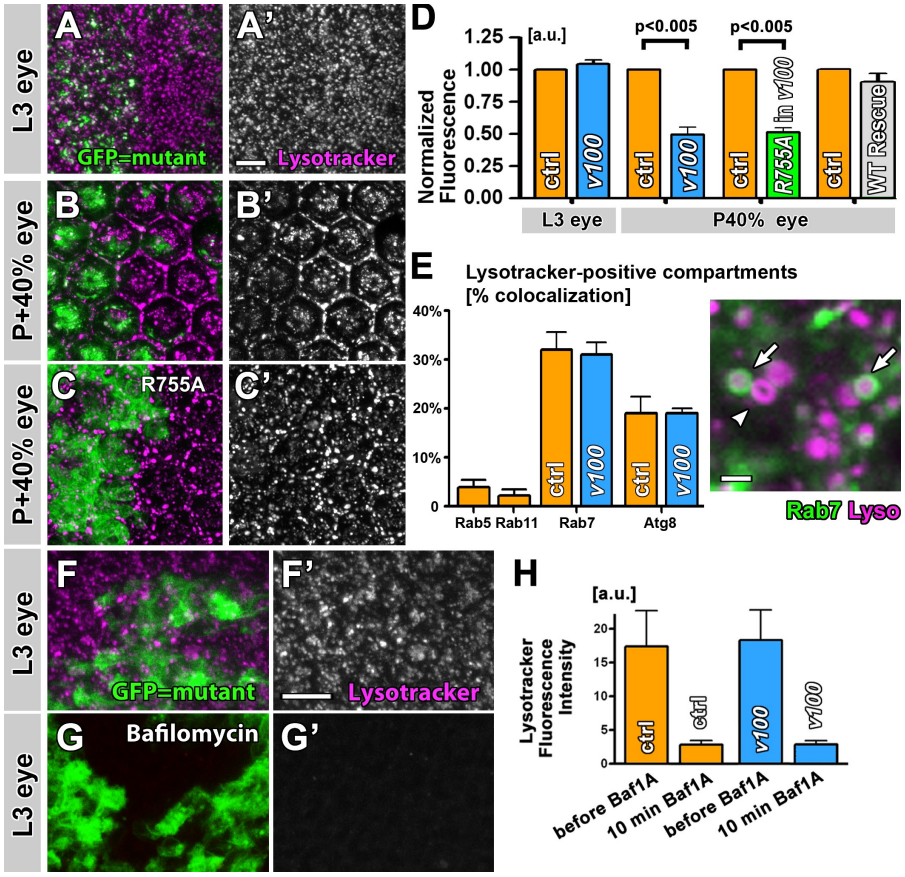

Figure 2. **V100 is required for the acidification of a subset of neuronal degradative compartments.** (A–C′) Lysotracker live measurements in eye–brain cultures. (A and B) Representative scans of *v100* MARCM eye discs (mutant cells marked with GFP). (A′ and B′) Only Lysotracker channel. (C) Live scan of a *v100* MARCM eye expressing $v100^{R755A}$ only in the mutant cells marked by GFP. (C′) Only Lysotracker channel. (D) Quantification of Lysotracker data in A–C′ shows a significant reduction in Lysotracker signal after photoreceptor differentiation at P + 40% (orange, control [ctrl]; blue, mutant). Expression of $v100^{R755A}$ in the mutant (green) does not rescue the Lysotracker signal reduction. Gray, expression of $v100^{WT}$ in mutant photoreceptors. (E) Identification of Lysotracker-positive compartments by live imaging using GFP-Rab5, GFP-Rab11, GFP-Rab7, and Atg8-GFP. Note that the ratio of Rab7/Lysotracker and Atg8/Lysotracker compartments is unaltered in the mutant despite the 50% Lysotracker reduction shown in D. The inset shows Rab7-positive late endosomes that are filled with Lysotracker (arrows). The arrowhead shows a Rab7-negative, lysotracker-positive ring, presumably a lysosomal or autophagosomal structure. (F–H) Block of all v-ATPase–dependent acidification using bafilomycin A1 in L3 larval eye discs with mutant *v100* MARCM clones marked by GFP. Error bars indicate SEM. Bars: (A′ and F′) 10 µm; (E) 1 µm.

Atg8-positive strongly acidified compartments is unaltered in the mutant (Fig. 2 E; and Fig. S1, E and F). Thus, neither compartment type is lost in the mutant. Instead, these findings indicate a loss of a neuronal subset of these compartment types. Collectively, our data suggest that V100 is required for the acidification of a neuronal subset of late endosomal and autophagosomal compartments and that this acidification function is not rescued by $v100^{R755A}$.

V100 is enriched on early endosomes

To comprehensively characterize V100-positive compartments in WT, we used a panel of 16 markers for colocalization analyses in developing and adult photoreceptors. We performed these experiments using high resolution 3D confocal microscopy that allows the visualization of distinct subcellular compartments at the resolution limit of light (Hiesinger et al., 2001). To quantify compartment colocalization, we identified clearly discernible intracellular V100-positive compartments and counted how many of these were positive for a given other intracellular compartment marker as shown in Fig. S2 (A–D) for the synaptic vesicle marker cystein string protein (CSP) and the late endosomal marker Rab7. As shown in Fig. 3 (A and B), WT V100 colocalizes to a varying degree with several markers of membrane compartments, including endosomes, lysosomes, and synaptic vesicles (Fig. 3 B, marked endo, lyso, and syn.ves.). Most strikingly, only immunolabeling of the early endosomal marker syntaxin7 (Syx7)/Avalanche (Avl) exhibits a localization pattern that is almost identical to V100 (Fig. 3, C and D). Syx7/Avl acts together with Rab5 in vesicular fusion with early endosomes (Lu and Bilder, 2005). Indeed, the second most colocalizing marker of V100-positive compartments is the early endosomal marker Rab5 (Fig. 3 B; and Fig. S3, E and F). This colocalization pattern is substantiated in a complementary experiment using photoreceptor-specific expression of GFP-Rab5 (Wucherpfennig et al., 2003). GFP-Rab5 exhibits strong labeling along the developing rhabdomeric structure in the cell bodies (Fig. 3 E, green arrowhead) as well as in photoreceptor axon terminals (Fig. 3 E, blue arrow). V100 immunolabeling colocalizes with GFP-Rab5 at the axon terminals (Fig. 3 E, blue arrow) but only little in the cell bodies (Fig. 3 E). These data suggest that V100 is enriched together with synaptic endosomes. In contrast, colabeling with the lysosomal marker Sun/CD63 (Xu et al., 2004) reveals little V100 colocalization and a converse distribution pattern (increased levels in the cell bodies [Fig. 3 E, red arrowhead] and very low levels in developing synaptic regions [Fig. 3 E]). Similarly, expression of fluorescently tagged V100 in *v100*-null mutant neurons (that rescues its function) reveals partial colocalization with the endosomal markers Hrs and Rab11 (Lloyd et al., 2002; Pelissier et al., 2003) but less colocalization with the lysosomal marker Spin/Bnch (Fig. S3, G–I; Sweeney and Davis, 2002; Dermaut et al., 2005). Collectively, our WT compartment characterization yields the surprising finding that V100 most strongly colocalizes with early endosome markers in addition to synaptic vesicles and exhibits comparably less colocalization with lysosomal markers.

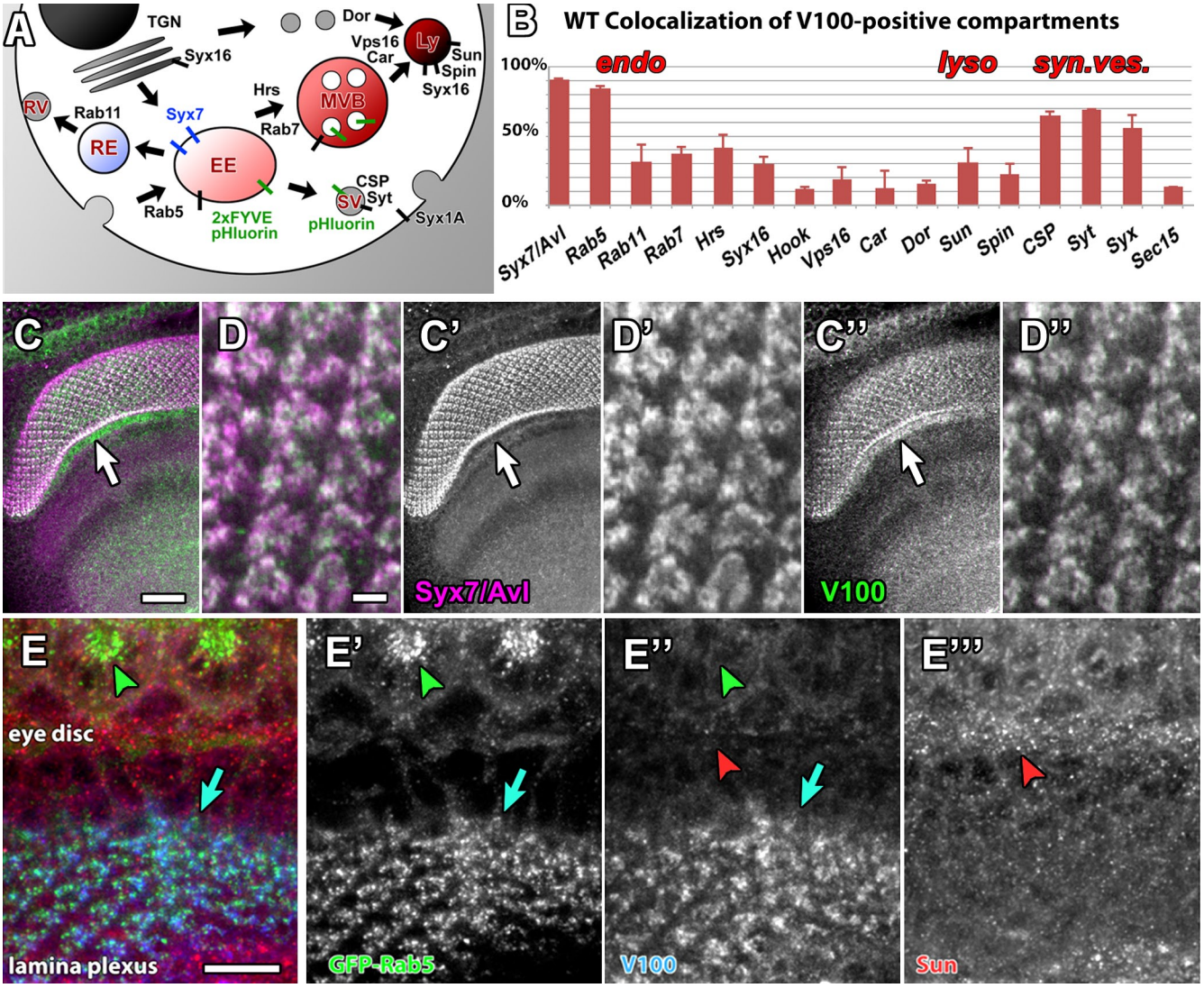

Figure 3. **V100 is predominantly an early endosomal protein in addition to its localization to synaptic vesicles.** (A) Schematic of intracellular localization of markers and compartments in WT. (B) WT colocalization of 16 markers with V100 in developing photoreceptor terminals at ~P + 25%. (C and D) Double labeling of a developing optic lobe for Syx7/Avl (purple) and V100 (green). (D) High resolution section of the developing lamina. Arrows in C indicate increased labeling of the lamina, which is shown at a higher resolution in D. (C'–D'') Single channels from C and D are shown. (E) Triple labeling of a developing eye–brain section. Green, photoreceptor-specific expression of Rab5-GFP; blue, V100; red, Sunglasses/CD63. Note that V100 and Rab5-GFP colocalize at the developing photoreceptor terminals (lamina plexus), whereas Rab5-GFP is also enriched at the developing rhabdomeres in the cell bodies (eye disc). Blue arrows show colocalization of GFP-Rab5 and V100 at synapses, green arrowheads indicate absence of colocalization of GFP-Rab5 and V100 at the rhabdomeres, and red arrowheads indicate absence of colocalization of Sun and V100. (E''') In contrast to V100, the lysosomal marker Sunglasses marks different compartments, mostly in the cell bodies. EE, early endosome; MVB, multivesicular body/late endosome; Ly, Lysosome; SV, synaptic vesicle; RE, recycling endosome; RV, recycling vesicle. Error bars indicate SEM. Bars: (C) 10 µm; (D) 1 µm; (E) 5 µm.

Loss of *v100* causes endosomal and autophagosomal accumulations

To understand the trafficking defects in *v100* mutant photoreceptors, we examined changes of the 16 intracellular compartment markers presented in the previous section. We again engineered MARCM flies in which 50% of all photoreceptors are rendered mutant and positively labeled with a fluorescent marker, whereas the other 50% serve as control in the same brain. As shown in Fig. 4 (A and B), photoreceptor terminals of 1-d-old adults exhibit up-regulation specifically of endosomal and lysosomal compartment markers. The most prominently up-regulated markers include the early endosomal Syx7/Avl, the early and late endosomal *rab* GTPases Rab5 and Rab7, and the lysosomal marker Sun/CD63. In contrast, markers for the synaptic target membrane Syx1A, the Golgi/lysosomal Syx16, and several other membrane proteins remain largely unaltered. Thus, we find up-regulation of specific markers along the endolysosomal pathway that suggest accumulations of both early and late endosomal compartments. Correspondingly, Western blot analysis of total protein extract from 2-d-old *v100* mutant eye–lamina complexes shows a clear increase of the endosomal proteins Syx7/Avl and Hrs (Fig. S3, A–C). These data support the idea of a protein degradation defect.

We have previously performed transmission electron microscopy of 1-d adult *v100* mutant photoreceptors. In our previous study, we found a significant increase of vesicular content

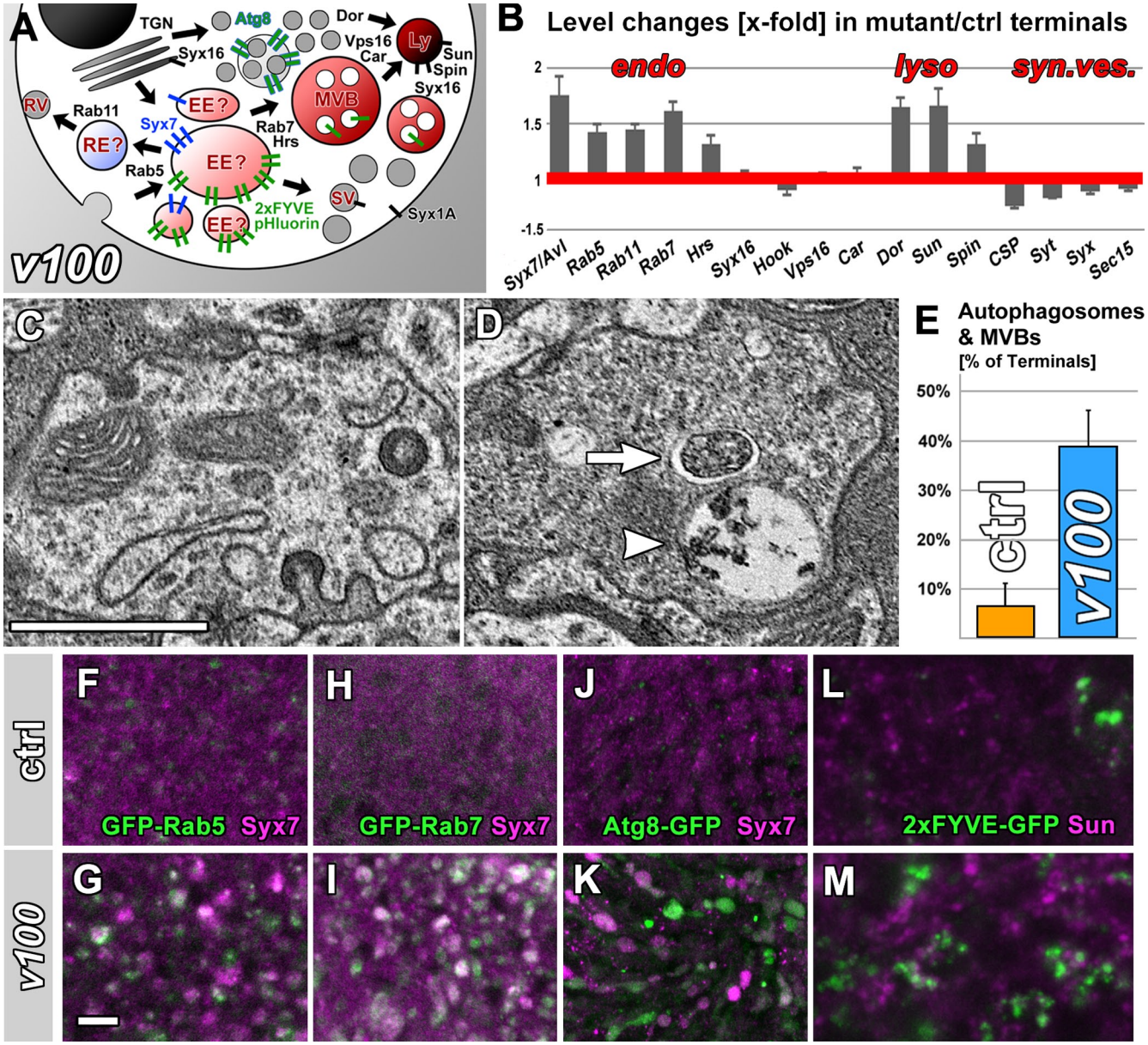

Figure 4. **Loss of *v100* causes endosomal and autophagic accumulations.** (A) Schematic of heterogeneous intracellular accumulations in the *v100* mutant. (B) Ratio of expression levels in mutant photoreceptor terminals compared with WT control (ctrl) in 50% mosaics. The red line represents unaltered levels. Note that numerous endosomal and lysosomal membrane markers are up-regulated. (C and D) Representative transmission electron micrographs reveal aberrant multivesicular structures and AVs (MVBs [arrowhead] and AVs [arrow]) in *v100* mutant photoreceptor terminals. (E) Quantification of MVB-like (single membrane) and AV-like (double membrane) structures per photoreceptor terminals show a more than fivefold increase in the mutant ($P < 0.01$). (F and G) Co-immunolabeling of early endosomes using Syx7 and Rab5 reveals strong up-regulation in mutant cells. (H and I) Coimmunolabeling of Syx7 and Rab7. (J and K) Colabeling of autophagosomes using Atg8-GFP and anti-Syx7 labeling reveals both makers accumulating in mostly separate compartments. (L and M) Colabeling of early endosomes using 2xFYVE-GFP and lysosomes using anti-Sunglasses reveals that both markers accumulate in mutually exclusive compartments. EE, early endosome; MVB, multivesicular body/late endosome; Ly, Lysosome; SV, synaptic vesicle; RE, recycling endosome; RV, recycling vesicle. Error bars indicate SEM. Bars: (C) 5 µm; (G) 1 µm.

but no alterations of active zones or mitochondria (Hiesinger et al., 2005). To identify ultrastructural correlates of the endo-lysosomal accumulations, we analyzed the transmission electron microscopy data for morphologically abnormal membranous compartments. As shown in Fig. 4 (C–E), quantitative analysis reveals a significant increase of highly heterogeneous enlarged structures, many of which appear morphologically as multivesicular bodies (MVBs; Fig. 4 D, arrowhead) or double-membrane autophagosomal vacuoles (AVs; Fig. 4, D [arrow] and E [quantification]). We did not observe any multilamellar structures that represent failed degradation in aberrant lysosomal structures, as are apparent for example in micrographs of photoreceptor terminals of the lysosomal storage mutant *spinster/bnch* (Dermaut et al., 2005). Instead, accumulations of both MVBs and AVs are indicative of compartments before lysosomal degradation.

Lastly, we performed a series of experiments using fluorescent reporters of the different trafficking and degradation compartments. As a marker for MVBs, we used YFP-Rab7, for AVs,

LC3/dATG8-GFP, and for early endosomes, YFP-Rab5 and 2xFYVE-GFP. Expression of any of these four markers results in large accumulations in *v100* mutant 1-d adult photoreceptors (Fig. 4, F–M). Immunolabeling for Syx7 reveals substantial colocalization with endosomal Rab5, Rab7, and 2xFYVE accumulations (Fig. 4, F–I; and not depicted). In contrast, Atg8-positive autophagosomal compartments are mostly nonoverlapping with the Syx7-positive endosomal accumulations (Fig. 4, J and K). Similarly, both the early endosomal markers GFP-2xFYVE (Wucherpfennig et al., 2003) and the lysosomal marker Sun/CD63 (Xu et al., 2004) accumulate but do so in mutually exclusive compartments (Fig. 4, L and M). These data suggest that early endosomal markers, including Syx7, do not accumulate in a single type of Atg8-positive AV or Sun/CD63-positive lysosome. Instead, accumulations occur at the level of endosomes in addition to lysosomal and autophagosomal degradative compartments.

V100 exerts an acidification-independent function on early endosomes

The accumulation of late endosomes and autophagosomes is consistent with the acidification defects of late endosomal and autophagosomal compartments shown in Fig. 2. But why is V100 predominantly localized on early endosomes? Early endosomal compartments can mature into late endosomal compartments (Rink et al., 2005). V100 may thus exert an acidification-independent function on early endosomes that later mature into degradative compartments and require increased acidification. To assay how loss of *v100* affects the pH of endosomal compartments, we expressed the membrane-tagged fluorescent probe synapto-pHluorin (hereafter referred to as pHluorin) in photoreceptors. pHluorin is a genetically encoded pH-sensitive GFP variant that can be used to measure the pH of synaptic vesicles and other intracellular compartments (Ng et al., 2002). Synaptic vesicles and endocytic vesicles can fuse with endosomal compartments, and pHluorin was previously shown to localize to endosomes (Machen et al., 2003).

At WT photoreceptor synapses, pHluorin labeling is very similar to the synaptic vesicle marker CSP (Fig. 5 A). In addition, pHluorin marks regions enriched for the early endosomal marker Rab5 (Fig. S3 D) but colocalizes very little with the late endosomal marker Rab7 and the recycling endosomal marker Rab11 (unpublished data). Remarkably, in *v100* mutant terminals, the colocalization of pHluorin with the synaptic vesicle markers CSP is mostly lost (Fig. 5 B). Instead, accumulations of pHluorin partially colocalize with the early endosomal markers Syx7/Avl (Fig. 5 C) and Rab5, the late endosomal marker Rab7, and the recycling endosomal marker Rab11 (Fig. S3, E–G). Photoreceptor-specific expression of WT *v100* fully recues this phenotype (Fig. S3, H–K). These data indicate that pHluorin accumulates in *v100* mutant terminals in compartments along the endosomal pathway, including Syx7/Avl-positive endosomes.

To measure the acidification of these compartments, we again used the v-ATPase–specific inhibitor bafilomycin 1A. pHluorin has reduced fluorescence when exposed to acidic pH, and loss of acidification results in a fluorescence increase. In our photoreceptor preparation, the pharmacological block of all v-ATPase function leads to a 1.37-fold pHluorin fluorescence increase in the WT and a statistically not significantly different 1.42-fold increase in the mutant (Fig. 5, H–N). This finding indicates that pHluorin-positive compartments are acidified in *v100* mutant neurons. We further confirmed that pHluorin accumulates in acidified compartments in cell bodies and at synapses using a calibrated alkalization/acidification protocol based on NH_4Cl washes as described in Materials and methods and shown in Fig. S4 (A–D). Collectively, with the WT localization data, these findings suggest that V100 is an endosomal protein that is not required for endosomal acidification.

Next, we tested how $v100^{R755A}$ expression affects the pHluorin localization and measurements in *v100* mutant neurons. Surprisingly, fluorescence levels reveal a dramatic further increase of pHluorin accumulations in *v100* mutant photoreceptors expressing $v100^{R755A}$ compared with the mutant alone (Fig. 5, D–F; and Fig. S4 E). This finding follows the previously observed pattern of phenotypes worsened by $v100^{R755A}$ expression, namely ERG amplitude and cell death (Fig. 1). Because $v100^{R755A}$ expression causes massive photoreceptor cell loss only when expressed in null mutant photoreceptors (Fig. 1, G–I), we wondered whether the same is true for pHluorin accumulations. Fig. 5 G shows a mosaic of synaptic terminals of 1-d-old photoreceptors in which WT terminals are marked with RFP (Fig. 5 G, magenta), whereas the *v100*-null mutant terminals are unmarked. In addition, we co-expressed both $v100^{R755A}$ and pHluorin at identical levels in all photoreceptors. Remarkably, only $v100^{R755A}$ expression in *v100* mutant photoreceptors, but not in a WT control clone, causes dramatic pHluorin accumulations at the synaptic terminals (Fig. 5 G). This finding shows that the pHluorin accumulation phenotype indeed follows the same pattern as the reduction in ERG depolarization and eye size; in all cases, $v100^{R755A}$ causes more severe phenotypes in the absence of WT *v100*.

Finally, we performed acidification measurements using the aforementioned bafilomycin protocol. As shown in Fig. 5 (H–N), pharmacological block of all v-ATPase function in photoreceptors with $v100^{R755A}$ expression in a mutant background causes a 1.79-fold increase in fluorescence. This finding indicates that the increased accumulations occur in compartments that are at least as acidified as in WT and the null mutant (Fig. 5 N). Indeed, the 1.79-fold increase is significantly higher than in the null mutant, which is likely a result of the dramatic increase in the amount of pHluorin. The accumulation of pHluorin in acidified compartments was again confirmed using calibrated NH_4Cl washes (Fig. S4 E). Our findings support the notion that selective rescue of an acidification-independent function causes protein accumulations only when no WT protein provides acidification.

V100 interacts with the early endosomal Syx7/Avl but not the Golgi/lysosomal Syx16

Our findings raise the question about the molecular mechanism of the acidification-independent function. An important hint comes from the observation that V100 is an endosomal protein that is not required for endosomal acidification. We were intrigued by the Syx7 colocalization with V100 in WT as well as the Syx7 accumulation in the *v100* mutant because previous studies suggested acidification-independent functions of V100 and its homologues in

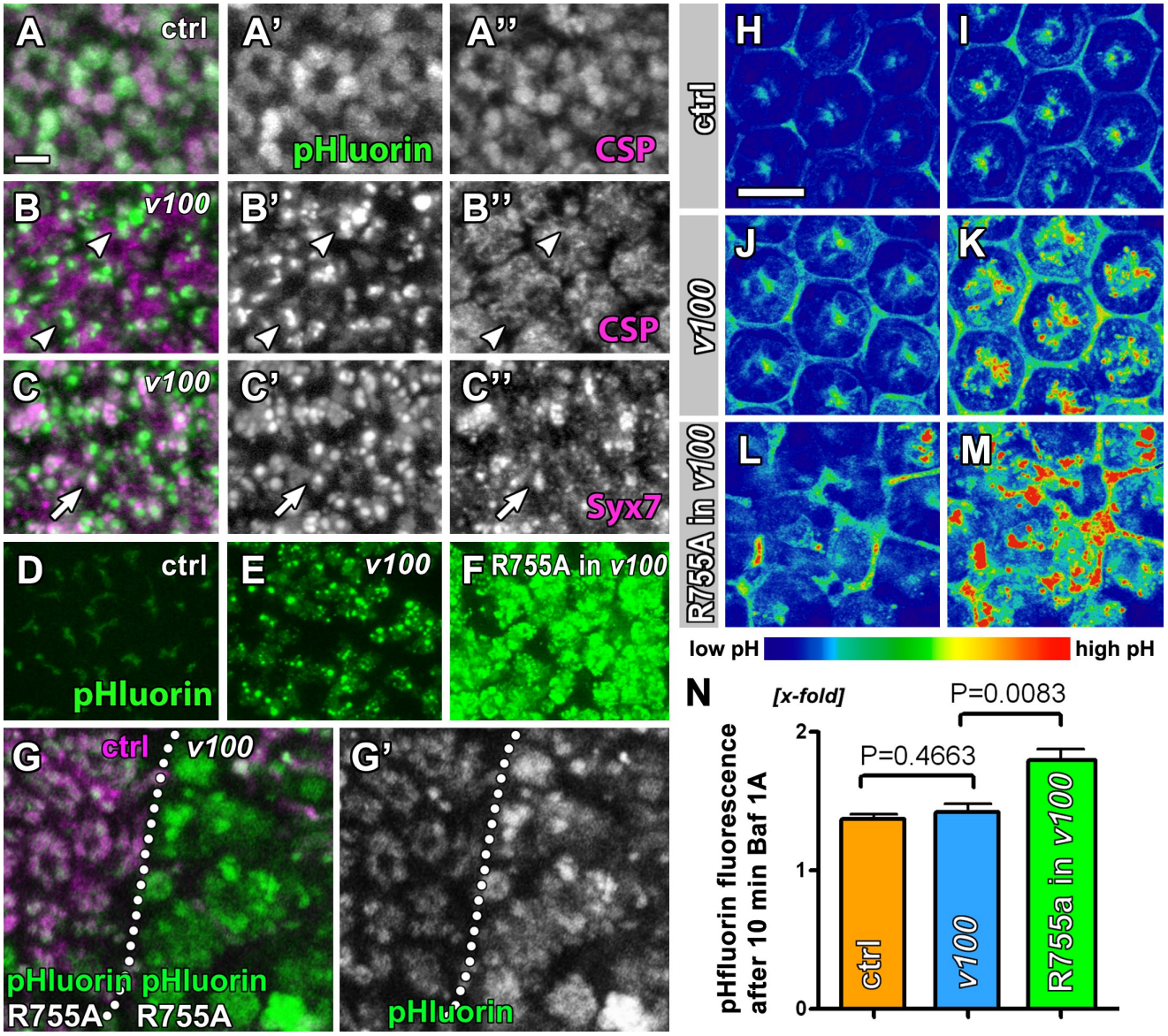

Figure 5. **V100 exerts an acidification-independent function on early endosomes.** (A–C″) High resolution section of WT (A) and *v100* mutant (B and C) 1-d adult photoreceptor terminals expressing pHluorin (green) and immunolabeled for CSP or Syx7/Avl (magenta). Note that pHluorin forms accumulations that exclude CSP (arrowheads) but partially colocalize with Syx7 (arrows) in the mutant. (D–F) Levels of pHluorin accumulation in live adult photoreceptor terminals at equal pH for the genotypes indicated. (G and G′) Negatively marked *v100* mutant clone (magenta, WT terminals). Both mutant and control (ctrl) clones equally overexpress pHluorin and $v100^{R755A}$. Note that $v100^{R755A}$ expression only in the mutant terminals leads to pHluorin accumulations. The dotted line approximates the clonal boundary. (H–M) Live confocal scans of P + 20% eye discs before and after 10-min incubation with the v-ATPase inhibitor bafilomycin 1A. (H and I) Control before and after bafilomycin treatment. (J and K) *v100* mutant before and after bafilomycin. (L and M) *v100* mutant with $v100^{R755A}$ rescue. (N) Quantification of fluorescence increases after bafilomycin treatment shows that pHluorin accumulates in compartments that are acidified in a v-ATPase–dependent manner. Error bars indicate SEM. Bars, 10 µm.

SNARE-mediated membrane fusion (Bayer et al., 2003; Hiesinger et al., 2005; Liégeois et al., 2006; Peri and Nüsslein-Volhard, 2008). Syntaxins are key SNARE proteins that mark specific target membranes where they are absolutely required for membrane fusion (Südhof and Rothman, 2009). Syx7/Avl is required for vesicle fusion with early endosomes in *Drosophila* (Lu and Bilder, 2005). In contrast, Syx16, which is located mostly at the Golgi and to some extent on lysosomes (Akbar et al., 2009), exhibits significantly less colocalization with V100 and no accumulation in the mutant (Fig. 3 B and Fig. 4 B). V100 directly binds to Syx1A (Syx1A), the target SNARE required for synaptic vesicle fusion (Hiesinger et al., 2005). To test a possible interaction of V100 with Syx7/Avl and Syx16, we performed coimmunoprecipitations (co-IPs) using the V100 antibody from fly heads. As shown in Fig. 6 A, some Syx7/Avl, but not Syx16, coimmunoprecipitates with V100. These results indicate that V100 exists in a complex with Syx7/Avl but not Syx16 in the brain. Conversely, V100 is coimmunoprecipitated with Syx7/Avl from brain extracts (Fig. 6 B). The amount of coimmunoprecipitated Syx7 was low compared with Syx1A (Fig. 6 A). To test the strength and specificity of these interactions, we performed a series of pull-down assays. First, we performed pull-downs from fly head extracts with His-tagged V100N (the N-terminal half of V100 that is unaffected by the R755A mutations) or His-tagged Syx7 and probed for Syx7 and V100,

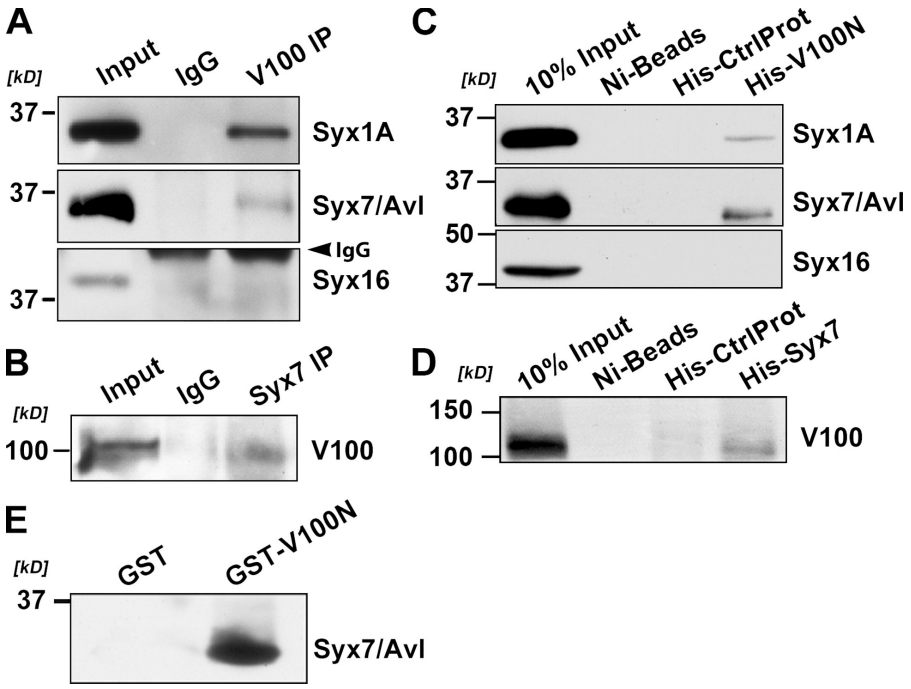

Figure 6. **V100 interacts with the endosomal Syx7/Avl but not the Golgi/lysosomal Syx16.** (A) Immunoblots of co-IP with anti-V100 antibody from adult fly head extract, probed with antibodies against Syx1A, Syx7/Avl, and Syx16. IgG, analogous co-IPs using preimmunoserum instead of anti-V100 serum. (B) Co-IP with anti-Syx7/Avl antibody from adult fly head extract probed with anti-V100. (C) Pull-down from adult fly head extract using bacterially made His-V100–N terminus. Immunoblot probed with anti-Syx1A, -Syx7, and -Syx16. (D) Pull-down from adult fly head extract using bacterially made His-Syx7. As negative control (His-CtrlProt), we used a bacterially made His fusion to a fly lipid enzyme (CG8630). Immunoblot probed with anti-V100. (E) GST pull-down of bacterially made His-Syx7 with bacterially made GST-V100–N terminus.

respectively. As shown in Fig. 6 (C and D), both proteins can pull down each other from brain extract robustly. This pull-down result is specific, as Syx7 and Syx1A, but not Syx16, are pulled down with V100N, corroborating the co-IP results (Fig. 6 D). Finally, because V100 is known to directly interact with Syx1A, we tested the direct interaction of bacterially synthesized and purified GST-tagged V100N with His-tagged Syx7. As shown in Fig. 6 E, V100 and Syx7 show strong, direct interaction. We conclude that V100 and Syx7/Avl robustly interact in vitro and in vivo. Note that the R755A mutation resides close to the C terminus of the 855–amino acid V100 protein, whereas the SNARE interaction motif resides in the N-terminal 140 amino acid (Hiesinger et al., 2005). As shown in this study, the unaltered N terminus is sufficient to bind to Syx7/Avl. Thus, these findings suggest a mechanistic basis for an acidification-independent function of V100 in vesicle fusion with target membranes marked by specific syntaxins.

Loss of *v100* causes slow, adult onset degeneration

Our data suggest that vesicle fusion with early endosomes in the $v100^{R755A}$ rescue leads to the fast accumulation of enlarged compartments that mature into degradation-incompetent compartments because of lack of acidification (Fig. 5, F, G, and M). In contrast, in the null mutant, we observe a much slower accumulation of degradation-incompetent compartments, as evidenced, for example, for pHluorin in Fig. 5 (E and K). If the accumulation of degradation-incompetent compartments is detrimental to cell viability, then the *v100*-null mutant might cause slow degeneration.

We previously reported synaptic transmission defects but no developmental or degenerative defects in embryos and adult *v100* mutant photoreceptors of 1-d-old flies (Hiesinger et al., 2005). Consistent with the previous findings, the depolarization of up to 1-wk-old *v100* mutant photoreceptors is indistinguishable from WT (Fig. 7, A and B). However, a weak reduction of the depolarization becomes apparent after 3 wk (Fig. 7, E and F) and progressively worsens by 5 wk (Fig. 7, I and J). All flies were raised in a 12-h light/12-h dark cycle. We also dark reared a set of control and *v100* mutant flies to investigate whether this reduction of photoreceptor responses is stimulus dependent. Dark-reared control flies exhibit a significantly increased depolarization (Fig. 7 M). The dark-reared mutants do not show this increase, but a depolarization that is not significantly different from 4–5-wk-old control flies raised in a normal light/dark cycle (Fig. 7 N). Fig. 7 Q summarizes these results quantitatively. Next, we analyzed the morphology of these eyes by immunolabeling with a monoclonal antibody against the transmembrane protein chaoptin that labels the rhabdomeres, i.e., the light-sensitive membrane organelles. In contrast to control flies, *v100* mutant photoreceptor cell bodies exhibit accumulations of chaoptin-positive structures while losing most discernible rhabdomeric structure by 5 wk (Fig. 7, K and L). Again, these phenotypes are progressive (compare with Fig. 7, C–L). Traditional plastic sections of these eyes further reveal the extent of the degenerative phenotypes with little discernible structures after 5 wk (Fig. S4, F and G). In 5-wk-old dark-reared mutants, aberrant chaoptin-positive accumulations are also apparent, but the rhabdomeric and overall structure are significantly less disrupted than in mutants after a 5-wk light/dark cycle (Fig. 7, O and P). Together, these data show a degenerative phenotype in *v100* mutant neurons that coincides with transmembrane protein accumulation, progresses slowly, and can be attenuated by absence of stimulation.

Selective rescue of the acidification-independent function accelerates degeneration by increasing accumulations in Syx7-positive, degradation-incompetent compartments

Our combined data support a model in which the acidification-defective $V100^{R755A}$ rescues vesicle fusion with the presynaptic

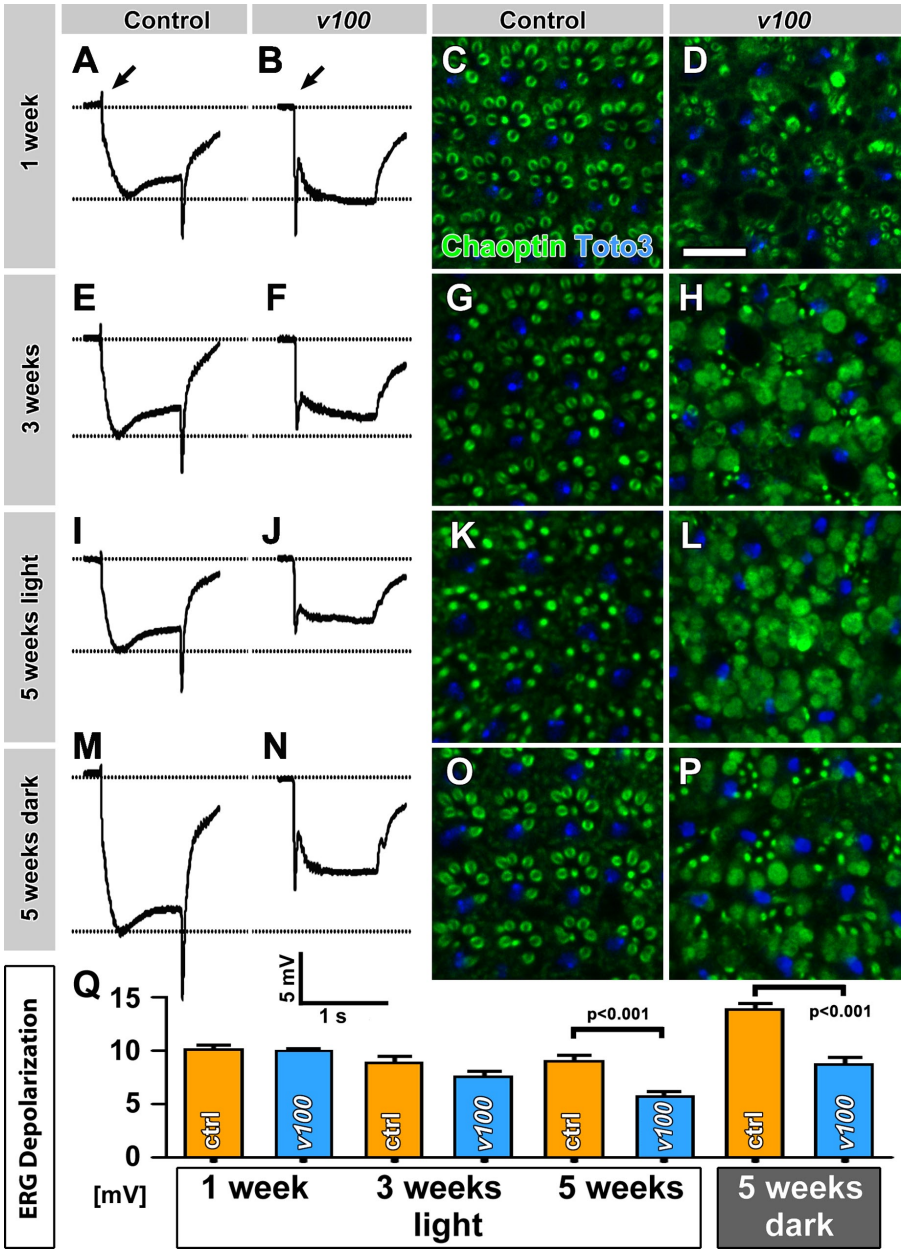

Figure 7. **Loss of *v100* causes slow, adult-onset neurodegeneration.** (A and B) ERG recordings of 1-wk-old flies. Note that mutant ERGs lack the on transient (arrows) but display normal depolarization. (C and D) Eyes from 1-wk-old WT and *v100* mutant flies labeled with the photoreceptor-specific rhabdomere marker chaoptin (green) and the nuclear marker Toto-3 (blue). (E and F) ERG recordings from 2–3-wk-old flies show a slight reduction in depolarization. (G and H) 2–3-wk-old WT and *v100* mutant eyes. (I–L) ERGs and immunolabeling of 5-wk-old WT and mutant eyes reveal progressive degeneration. (M–P) ERG recordings and immunolabelings from 5-wk-old flies kept in the dark show attenuated mutant phenotypes. (Q) Quantification for ERG depolarizations. Ctrl, control. Error bars indicate SEM. Bar, 10 µm.

membrane (via Syx1A interaction) and early endosomes (via Syx7 interaction; Fig. 8 A). In this model, rescue with $v100^{R755A}$ effectively speeds up cargo overload in degradation-incompetent compartments. Our model predicts that chaoptin, which accumulates slowly in null mutant photoreceptors (Fig. 7), accumulates faster in Syx7-positive compartments in the $v100^{R755A}$ rescue. As shown in Fig. 8 (B–D), in 1-d adult synaptic terminals of the null mutant, chaoptin exhibits small accumulations that are partially associated with Syx7 accumulations but mostly Syx7 negative. In contrast, $v100^{R755A}$ rescue of the null mutant at the same time point exhibits a dramatic increase of chaoptin accumulations in large vesicles that are invariably enclosed by large Syx7-positive compartments (Fig. 8 D, arrows; and Fig. S5, F–I, schematic). This observation supports the idea that $V100^{R755A}$ promotes the fusion of cargo vesicles with Syx7-positive endosomes.

Finally, our model predicts a dominant function of $V100^{R755A}$ that is different from the loss of function phenotype but consistent with the ERG defects shown in Fig. 1 (B–D). Therefore, we analyzed the effect of $v100^{R755A}$ overexpression on photoreceptor morphology and degeneration in 2-wk-old flies. As shown in the previous section, loss of *v100* causes slow neurodegeneration that is accompanied by accumulations of chaoptin (Fig. 7 and Fig. S5 A). This phenotype is rescued by *v100* expression in mutant photoreceptors (Fig. S5 B). Overexpression of WT *v100* causes no obvious defects (Fig. S5 C). In contrast, overexpression of $v100^{R755A}$ in WT photoreceptors causes the accumulation of Syx7 at the base of rhabdomeres (Fig. S5 D, arrows) but no apparent accumulation of chaoptin and no degeneration of the rhabdomeric structure (Fig. S5, B–D, arrowheads). These observations are consistent with a mild dominant effect of $v100^{R755A}$ that is distinct from the null

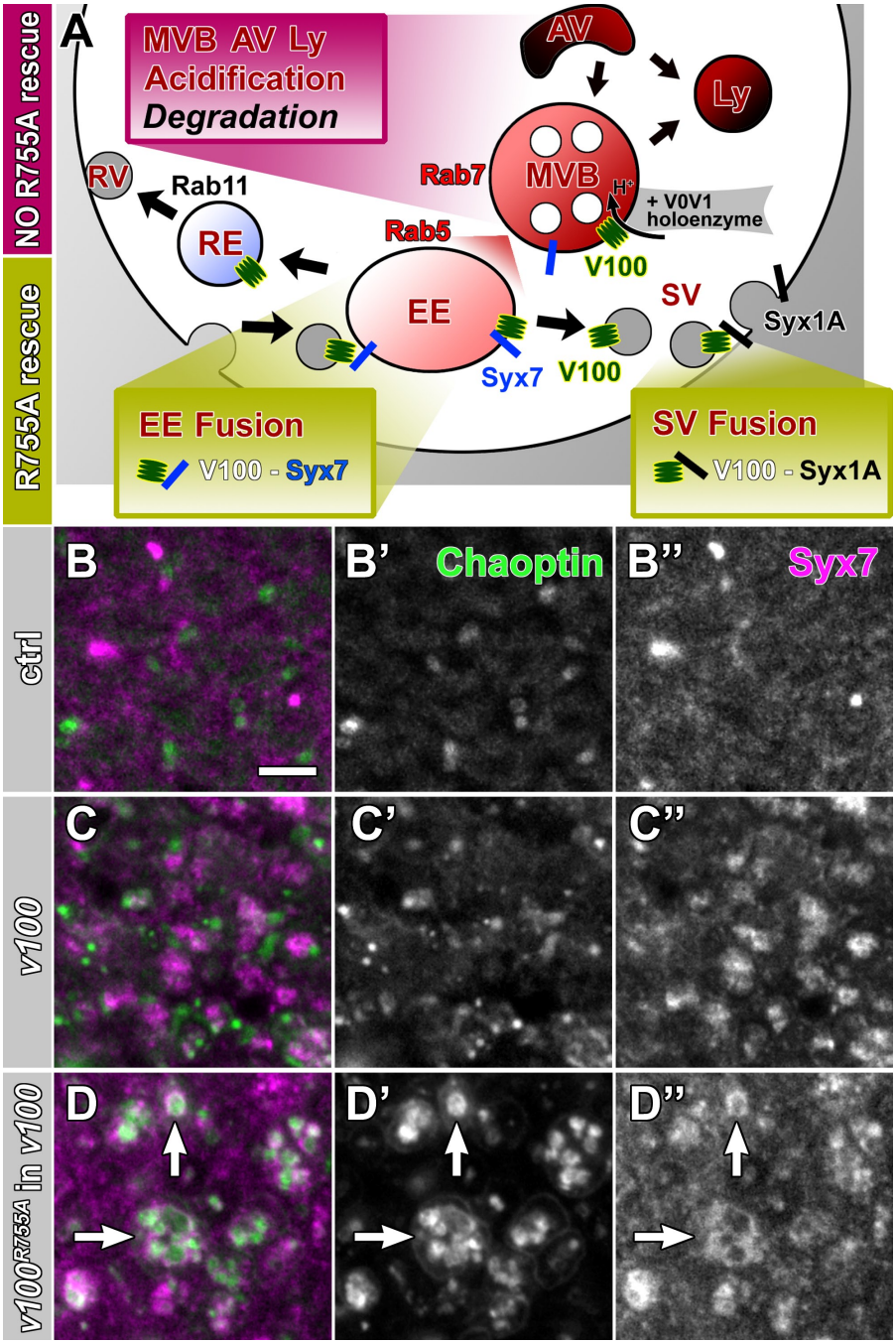

Figure 8. **Selective rescue of the acidification-independent function accelerates degeneration by increasing accumulations in Syx7-positive, degradation-incompetent compartments.** (A) Summary of V100 functions and $v100^{R755A}$ rescue data. Our findings indicate two acidification-independent functions that are rescued by $v100^{R755A}$: synaptic vesicle (SV) fusion through Syx1A interaction and early endosomal (EE) fusion through Syx7 interaction. In contrast, V100 has a function as part of the V0V1 holoenzyme once endosomes mature into degradative compartments that are not rescued by $v100^{R755A}$. Consequently, selective rescue of the acidification-independent function leads to increased accumulations in Syx7-positive, degradation-incompetent compartments. (B, C, and D) 1-d adult photoreceptor terminals for control (B), *v100*-null mutant (C), and $v100^{R755A}$ rescue in the *v100* mutant (D). (B′, C′, and D′) Chaoptin alone (green channel) is shown. (B″, C″, and D″) Syx7 alone (magenta channel) is shown. In the $v100^{R755A}$ rescue, most chaoptin accumulates in large, Syx7-encircled MVB-like structures (arrows). RE, recycling endosome; RV, recycling vesicle. Bar, 5 µm.

mutant phenotype (compare with Fig. S5, G and H). Finally, expression of $v100^{R755A}$ in null mutant photoreceptors causes dramatically "blown-up" accumulations that appear like exacerbated versions of those in the null mutant (Fig. S5, E and I). These data suggest that $v100^{R755A}$ in WT photoreceptors causes mild intracellular accumulations and no degeneration, whereas $v100^{R755A}$ in mutant photoreceptors greatly exacerbates the null mutant phenotype.

Discussion

In this study, we characterize an integrated dual function of V100, the neuron-specific V0-ATPase subunit a1 in *Drosophila*. The genetic dissection of two molecularly distinct functions of *v100* suggests one role of V100 in endosomal vesicle fusion, and a second role in acidification downstream of endosomal sorting. Our data support an acidification-independent function in promoting vesicle fusion with target membranes marked by specific syntaxins that explains both V100's role in endosomes presented in this study as well as in synaptic vesicle exocytosis reported previously (Fig. 8 A; Hiesinger et al., 2005). Importantly, *v100* is only required in neurons after neuronal differentiation; general cellular functions that require essential endolysosomal trafficking are unaffected. We conclude that V100 provides a neuronal degradation mechanism whose loss leads to neurodegeneration.

Genetic dissection of the dual function

We propose the following model based on V100's dual function (Fig. 8 A and Fig. S5). In the absence of V100, vesicles with heterogeneous cargo, either endocytosed or ER/Golgi derived, fail to fuse with Syx7-positive endosomes, resulting in intracellular accumulations (Fig. S5, F and G). Over time, many of these accumulations are engulfed by AVs. V100-dependent acidification is required, and possibly acts as a trigger, for the subsequent maturation and degradation of MVBs and AVs. Expression of *v100*^{R755A} does not rescue acidification-dependent degradation in *v100*-null mutant neurons but promotes fusion of cargo vesicles with endosomes that thereby contain acidification-defective v-ATPases. In a WT background, the presence of WT V100 provides some acidification for the degradation of cargo (Fig. S5 H), whereas in a mutant background, this rerouting of cargo leads to dramatically increased MVB and AV formation (Fig. S5 I).

V0 and V1 sector assembly is thought to be a regulatory mechanism that initiates acidification (Nishi and Forgac, 2002; Marshansky and Futai, 2008). The reversible assembly of the V0V1 holoenzyme provides an elegant mechanism for the integration of V100's dual function. V100 is the largest component of the V0 membrane complex, and its N terminus is potentially free to interact with syntaxins when the two sectors are disassembled.

We have no evidence that the acidification function of *v100* is required for neurotransmitter release. In fact, neurotransmitter release in photoreceptors is the only phenotype that is rescued with the acidification-disrupted V100^{R755A}. In contrast, the neuron-specific endolysosomal trafficking defects described in this study are best explained in the context of two distinct molecular functions. Notably, V100 is localized to both synaptic vesicles and endosomes but is not required for the acidification of either of these organelles (Fig. 8 A). In addition, we have previously shown that *Drosophila* V100 can rescue a vesicle trafficking, but not an acidification defect of its orthologue *vph1* in yeast (Hiesinger et al., 2005). It is possible that a conserved acidification-independent function of *vph1* can be rescued in a trans-species experiment with *v100* in yeast, whereas the V0V1-holoenzyme–dependent acidification function is not as easily rescued.

What is the mechanism of the acidification-independent function of V100? We report in this study that V100 specifically interacts with syntaxins on membranes where its function is most consistent with the promotion of membrane fusion: synaptic vesicle fusion with presynaptic membranes marked by Syx1A and endosomal fusion with membranes marked by Syx7. These results suggest a novel role for V100 and its homologues in targeting or increasing the fusion probability of vesicles marked with different compartment-specific subunit a1–a4 homologues and their respective target membranes. This function would be consistent with a role of V100 before or during SNARE-mediated membrane fusion.

A neuronal "sort and degrade" mechanism

We show that *v100* is not required for the acidification of some of the compartments in which cargo (e.g., pHluorin or chaoptin) accumulates. The observation that selective rescue of an acidification-independent sorting function causes more accumulation than the null mutant alone implies that degradation in *v100* mutant neurons is only partly abolished. In other words, loss of *v100* does not affect at least one other v-ATPase (i.e., bafilomycin sensitive and a2–a4 dependent) degradation pathway. The presence of at least one other degradation pathway is further supported by the presence of a normal number of strongly acidified degradative (Lysotracker positive) compartments in the mutant cells before neuronal differentiation. Together with the WT expression data, our results indicate that *v100* only comes into play after a cell has adopted the neuronal cell fate. Finally, the idea that essential endolysosomal function is unaffected in *v100* mutant neurons is also supported by the observation that *v100* mutant neurons lack several hallmarks of general lysosomal degradation mutants, including accumulations of autofluorescent lipofuscin or ceroid (Futerman and van Meer, 2004). Together, these data suggest that V100 is not required for all endolysosomal degradation in neurons. The *v100*-dependent mechanism need not be different from the essential endolysosomal pathway in any component other than *v100* itself; V100 promotes fusion with endosomes, which it later acidifies for degradation. Collectively, these data suggest that sorting and degradation are tightly balanced.

v100 is required only in neurons in *Drosophila* and is at least strongly enriched in the nervous system of all animals investigated for it. However, the temporally integrated mechanism of sort and degrade that we describe in this study could be more general. All a1–a4 homologues are highly conserved, and acidification-independent roles in secretion have been suggested for a2 in *C. elegans* (Liégeois et al., 2006) and a3 in mouse (Sun-Wada et al., 2006). The zebrafish a1 orthologue has an acidification-independent function in phagosome–lysosome fusion in microglial cells (Peri and Nüsslein-Volhard, 2008). Thus, it is possible that the mechanism we describe in this study for neurons may be used by other cell types.

Neuronal endolysosomal trafficking, autophagy, and neurodegeneration

Loss of *v100* leads to heterogeneous accumulations of endosomal compartments, MVBs, and AVs. Autophagy intersects at many levels with the classical endolysosomal pathway: fusion of AVs with lysosomes, MVBs, and early endosomes are known to form amphisomal compartments and have been shown to be required for autophagic function (Eskelinen, 2005; Filimonenko et al., 2007; Razi et al., 2009). Numerous mutants in endolysosomal and autophagic pathways lead to late onset neurodegeneration (Futerman and van Meer, 2004; Hara et al., 2006; Komatsu et al., 2006). Conversely, induction of autophagy can alleviate neurodegenerative effects (Mizushima et al., 2008; Wang et al., 2009). Similarly, our findings are consistent with the idea that loss of degradation capacity sensitizes neurons to cargo overload. In support of this idea, overexpression of human disease proteins (including Aβ and τ) exhibit significantly accelerated neurodegeneration in *v100* mutant photoreceptors (unpublished data). The recognition of a neuronal mechanism that operates in addition to essential degradation mechanisms may be an important parameter to consider in neuronal diseases associated with undegraded protein accumulations.

Materials and methods

Genetics, molecular biology, and generation of transgenic flies

v100-null mutant and overexpression lines have been described previously (Hiesinger et al., 2005). Allele $v100^4$ was the mutant allele used in all experiments. *v100* was subjected to site-directed mutagenesis using full-length *v100* cDNA in a pOT2 vector (BDGP clone LD21248) and the primer 5′-CACCGCTTCCTATCTGGCATTGTGGGCGCTTTCCT-3′ and its reverse complement. Introduction of the mutation R755A was verified by sequencing. The resulting $v100^{R755A}$ cDNA was cloned into pUAST using EcoRI and XhoI restriction cutting sites as reported previously (Hiesinger et al., 2005). The UAS-Dendra2-*v100* construct was generated by cloning the PCR-amplified Dendra2 open reading frame into the pENTR4 vector and generating the fusion using the Gateway system. DNA injection for the generation of transgenic flies was performed by Rainbow Transgenics, Inc. At least two independent transgene insertions per chromosome were isolated. Two independent insertions for both $v100^{R755A}$ and Dendra2-*v100* on the second chromosome were tested and selected for comparable expression levels with the UAS-*v100* WT insertion when expressed in photoreceptors. The two transgenic lines chosen for each construct behaved identical in all assays.

Immunohistochemistry, microscopy, and image processing

Adult brains, eyes, and eye–lamina complexes as well a pupal brains and eye–brain complexes were dissected as reported previously (Williamson and Hiesinger, 2010). The tissues were fixed in PBS with 3.5% formaldehyde for 15 min and washed in PBS with 0.4% Triton X-100. High resolution light microscopy was performed using a resonance-scanning confocal microscope (SP5; Leica). Imaging data were processed and quantified using Amira 5.2 (Indeed) and Photoshop (CS4; Adobe). Fluorescence data and ERG data were quantified using Prism (version 4; GraphPad Software, Inc.). Eye pictures were captured on a stereoscope (MX16F; Leica) using In-Focus (version 1.60; Meyer Instruments) and were processed for extended depth of field using Image-Pro Plus (version 6.0; Media Cybernetics). The following antibodies were used at 1:1,000 dilution: Syx7/Avl, Rab5, Rab7, Rab11, Hrs, Syx16, Hook, Vps16, Car, Dor, Sun, Spin, and Syt. Anti-chaoptin, anti-CSP, and anti-Syx were used at 1:50, and anti-Sec15 and anti-V100 were used at 1:2,000.

ERGs

ERGs were performed as described previously (Fabian-Fine et al., 2003) with the following modifications: flies were fixed using nontoxic Glue-All (Elmer's). We used 2 M NaCl in the recording and reference electrodes. Electrode voltage was amplified by a Digidata 1440A (MDS Analytical Technologies), filtered through an electrometer (IE-210; Warner Instruments), and recorded using Clampex (version 10.1; Axon Instruments). A postrecording filter was also provided by the Clampex software. Light stimulus was provided in 1-s pulses by a computer-controlled white light-emitting diode system (MC1500; Schott).

Protein interaction

Total proteins were extracted from adult fly heads in IP buffer containing 20 mM Tris, 150 mM NaCl, 1 mM PMSF, and 1× complete protease inhibitors (Roche), pH 7.4. The fly head extract was mixed well in 1% Triton X-100 (Bio-Rad Laboratories) and incubated for 1 h at 4°C. Samples were centrifuged at 16,000 *g* for 15 min at 4°C to remove cell debris. The resulting supernatant was incubated with 20 µl anti-V100 antibody (Hiesinger et al., 2005) coupled to protein A/G beads (Santa Cruz Biotechnology, Inc.) for 1 h at 4°C. After removing the supernatant, the beads were washed four times with IP buffer. The immunoprecipitates were eluted by boiling the beads in 50 µl SDS sample buffer and were analyzed by Western blotting. A nonspecific preimmune serum was used as control. Pull-down from adult fly head protein extract was performed using His-V100–N terminus or His-Syx7 as baits that were immobilized on Ni-charged beads (EMD). Bound proteins were eluted with SDS sample buffer and analyzed by Western blotting. Pull-down of bacterially produced proteins was performed using immobilized GST-V100–N terminus fusion protein as bait, which was then incubated with His-Syx7 for 1 h at 4°C in binding buffer (20 mM Tris, 100 mM NaCl, 1 mM EDTA, and 0.2% Triton X-100, pH 7.4). After washing with binding buffer four times, the bound proteins were eluted with SDS sample buffer and analyzed by Western blotting.

Western blots of mutant eye–lamina complexes

For Western blots of adult eye–lamina complexes, 2-d-old *ey*FLP; FRT82B *v100* and *ey*FLP; FRT82B WT eyes were dissected in HL3 as described previously (Williamson and Hiesinger, 2010). Tissues were washed twice in ice-cold lysis buffer (as used for IP experiments) and crushed with a pestle in lysis buffer. The solution was incubated on ice for 20 min and centrifuged at 4°C to remove solid material. 10 eye–lamina complexes per lane were run on a 12% SDS-PAGE gel.

Live imaging

Brains were dissected from either pharate adults or P + 20% pupae in HL3 and were immobilized on a coverslip coated with sylgard using glue stitch as described previously (Williamson and Hiesinger, 2010). The tissue was mounted in an orientation that allows imaging of the desired region. The coverslip was placed in a perfusion chamber (RC-30; Harvard) with slow perfusion of HL3 solution. Images were captured using resonance-scanning confocal microscopy. For each scan from individual experiments, the same x/y region was captured.

pHluorin. We generated a calibration curve by first alkalizing intracellular compartments using NH_4Cl, pH 7, and subsequently progressively acidifying intracellular compartments using an acidification protocol modified from Boron and De Weer (1976) by reducing the amount of free extracellular NH_3 using NH_4Cl washes, pH 6.5, 6.0, and 5.5. Using this method, the calibrated initial live measurements report intracompartmental pH, independent of the total amount of pHluorin. The raw data were processed in Amira (version 5.2; Visage Imaging GmbH) by first generating a maximum projection to eliminate the problem that differences in fluorescence vary among scans from a single experiment simply as a result of a slight shifting of the prep in the z direction resulting from perfusion of fluids over living tissue. Total fluorescence for each scan within a single experiment was calculated, and the scans from NH_4Cl (pH controlled) scans were plotted in Prism on a Kaplan–Meier survival curve and analyzed by the four-parameter logistic equation. Next, the live fluorescence measurement was mathematically fitted onto the curve to reveal the mean live pH of the environment to which pHluorin was exposed. This was performed for several animals, and the results were compiled to generate bar graphs representing the mean pH and error from the specified genotypes, tissues, and ages.

Lysotracker. For Lysotracker (Invitrogen) experiments, brains were removed from the animal and immobilized on a Sylgard-coated microscope slide using glue stitch. Lysotracker red was added to HL3 at 50 nM. 200 µl of this solution was placed onto the prepared tissue, and an image was acquired within 5 min, as recommended by the manufacturer to prevent alkalizing effects.

Quantification of compartment marker analyses

Up-/down-regulation in mutant versus WT photoreceptor terminals. 50% mutant photoreceptor mosaics were created with all mutant photoreceptors expressing pHluorin just to mark the mutant cells. 3D confocal stacks of three to five specimens were quantified for the ratio of total fluorescence in 3 μm^3 mutant terminals divided by total fluorescence in 3 μm^3 WT terminals for each of the 20 markers individually.

WT colocalization. Anti-V100 immunolabeling was analyzed for at least three specimens per colocalization experiment. Colabelings with guinea pig antibodies (anti-Hrs, -Dor, and -Sec15) were generated using GMR-GAL4–driven fluorescently tagged and functionally rescuing V100 in *v100* mutant neurons. For each colabeling experiment, clear and distinct V100-positive compartments were selected blindly with no other channel visible. Each V100-positive compartment was subsequently manually analyzed for colocalization with each of the 16 markers individually.

Plastic eye sections

1-µm plastic sections of adult eyes were made as described previously (Van Vactor et al., 1991). In brief, samples were fixed using standard electron microscopy fixatives containing 2% paraformaldehyde and 2% glutaraldehyde. Samples were subsequently dehydrated and embedded in epon/araldite plastic medium. Thick sections were stained with a combination of methylene blue and toluidine blue for light microscopy.

Online supplemental material

Fig. S1 shows Lysotracker labels late endosomal and autophagosomal compartments that are acidified in a v-ATPase–dependent manner. Fig. S2 shows high resolution 3D colocalization experiments of intracellular compartment marker colocalization. V100 colocalizes with endosomal markers but not the lysosomal protein Spin/Bnch. Fig. S3 shows endosomal defects: the endosomal proteins Syx7 and Hrs exhibit elevated protein levels in *v100* mutant eye–lamina complexes, and pHluorin accumulates in endosomal compartments. Fig. S4 shows eye defects: calibrated NH_4Cl washes reveal pHluorin accumulations in acidified endosomes. 5-wk-old *v100* mutant eyes

display almost complete loss of discernible structure. Fig. S5 shows that $V100^{R755A}$ expression causes a dominant defect that is different from the null mutant. Online supplemental material is available at http://www.jcb.org/cgi/content/full/jcb.201003062/DC1.

We would like to thank Helmut Krämer, Thomas Neufeld, Hugo Bellen, Bill Trimble, Matt Scott, Damian Crowther, Grace Zhai, Craig Montell, the Bloomington Stock Center, and the University of Iowa Developmental Studies Hybridoma Bank for reagents. We are especially grateful to Sanchali Ray and Helmut Krämer for providing the eye sections shown in Fig. S4. We further thank Michael Buszczak, Bassem Hassan, Ilya Bezprozvanny, Nikos Giagtzoglou, Nevine Shalaby, Grace Zhai, Tanja Rosenmund, Christian Rosenmund, Hugo Bellen, Sean Sweeney, and the members of the Hiesinger lab for discussion or critical comments on this or earlier versions of this manuscript.

This work was supported by grants from the National Institutes of Health (RO1EY018884 and RO1GM088803), the Welch Foundation (I-1657), the Whitehall Foundation, and the American Federation for Aging Research. P.R. Hiesinger is a Eugene McDermott Scholar in Biomedical Research.

Submitted: 12 March 2010
Accepted: 29 April 2010

References

Akbar, M.A., S. Ray, and H. Krämer. 2009. The SM protein Car/Vps33A regulates SNARE-mediated trafficking to lysosomes and lysosome-related organelles. *Mol. Biol. Cell.* 20:1705–1714. doi:10.1091/mbc.E08-03-0282

Bayer, M.J., C. Reese, S. Buhler, C. Peters, and A. Mayer. 2003. Vacuole membrane fusion: V0 functions after trans-SNARE pairing and is coupled to the Ca2+-releasing channel. *J. Cell Biol.* 162:211–222. doi:10.1083/jcb.200212004

Boron, W.F., and P. De Weer. 1976. Intracellular pH transients in squid giant axons caused by CO2, NH3, and metabolic inhibitors. *J. Gen. Physiol.* 67:91–112. doi:10.1085/jgp.67.1.91

Brand, A.H., and N. Perrimon. 1993. Targeted gene expression as a means of altering cell fates and generating dominant phenotypes. *Development.* 118:401–415.

Chang, Y.Y., and T.P. Neufeld. 2009. An Atg1/Atg13 complex with multiple roles in TOR-mediated autophagy regulation. *Mol. Biol. Cell.* 20:2004–2014. doi:10.1091/mbc.E08-12-1250

Dermaut, B., K.K. Norga, A. Kania, P. Verstreken, H. Pan, Y. Zhou, P. Callaerts, and H.J. Bellen. 2005. Aberrant lysosomal carbohydrate storage accompanies endocytic defects and neurodegeneration in *Drosophila* benchwarmer. *J. Cell Biol.* 170:127–139. doi:10.1083/jcb.200412001

Eskelinen, E.L. 2005. Maturation of autophagic vacuoles in Mammalian cells. *Autophagy.* 1:1–10. doi:10.4161/auto.1.1.1270

Fabian-Fine, R., P. Verstreken, P.R. Hiesinger, J.A. Horne, R. Kostyleva, Y. Zhou, H.J. Bellen, and I.A. Meinertzhagen. 2003. Endophilin promotes a late step in endocytosis at glial invaginations in *Drosophila* photoreceptor terminals. *J. Neurosci.* 23:10732–10744.

Filimonenko, M., S. Stuffers, C. Raiborg, A. Yamamoto, L. Malerød, E.M. Fisher, A. Isaacs, A. Brech, H. Stenmark, and A. Simonsen. 2007. Functional multivesicular bodies are required for autophagic clearance of protein aggregates associated with neurodegenerative disease. *J. Cell Biol.* 179:485–500. doi:10.1083/jcb.200702115

Futerman, A.H., and G. van Meer. 2004. The cell biology of lysosomal storage disorders. *Nat. Rev. Mol. Cell Biol.* 5:554–565. doi:10.1038/nrm1423

Hara, T., K. Nakamura, M. Matsui, A. Yamamoto, Y. Nakahara, R. Suzuki-Migishima, M. Yokoyama, K. Mishima, I. Saito, H. Okano, and N. Mizushima. 2006. Suppression of basal autophagy in neural cells causes neurodegenerative disease in mice. *Nature.* 441:885–889. doi:10.1038/nature04724

Hiesinger, P.R., M. Scholz, I.A. Meinertzhagen, K.F. Fischbach, and K. Obermayer. 2001. Visualization of synaptic markers in the optic neuropils of *Drosophila* using a new constrained deconvolution method. *J. Comp. Neurol.* 429:277–288. doi:10.1002/1096-9861(20000108)429:2<277::AID-CNE8>3.0.CO;2-8

Hiesinger, P.R., A. Fayyazuddin, S.Q. Mehta, T. Rosenmund, K.L. Schulze, R.G. Zhai, P. Verstreken, Y. Cao, Y. Zhou, J. Kunz, and H.J. Bellen. 2005. The v-ATPase V0 subunit a1 is required for a late step in synaptic vesicle exocytosis in *Drosophila. Cell.* 121:607–620. doi:10.1016/j.cell.2005.03.012

Kane, P.M. 2007. The long physiological reach of the yeast vacuolar H+-ATPase. *J. Bioenerg. Biomembr.* 39:415–421. doi:10.1007/s10863-007-9112-z

Kawasaki-Nishi, S., T. Nishi, and M. Forgac. 2001. Arg-735 of the 100-kDa subunit a of the yeast V-ATPase is essential for proton translocation. *Proc. Natl. Acad. Sci. USA.* 98:12397–12402. doi:10.1073/pnas.221291798

Kolotuev, I., A. Apaydin, and M. Labouesse. 2009. Secretion of Hedgehog-related peptides and WNT during *Caenorhabditis elegans* development. *Traffic.* 10:803–810.

Komatsu, M., S. Waguri, T. Chiba, S. Murata, J. Iwata, I. Tanida, T. Ueno, M. Koike, Y. Uchiyama, E. Kominami, and K. Tanaka. 2006. Loss of autophagy in the central nervous system causes neurodegeneration in mice. *Nature.* 441:880–884. doi:10.1038/nature04723

Kornak, U., A. Schulz, W. Friedrich, S. Uhlhaas, B. Kremens, T. Voit, C. Hasan, U. Bode, T.J. Jentsch, and C. Kubisch. 2000. Mutations in the a3 subunit of the vacuolar H(+)-ATPase cause infantile malignant osteopetrosis. *Hum. Mol. Genet.* 9:2059–2063. doi:10.1093/hmg/9.13.2059

Kornak, U., E. Reynders, A. Dimopoulou, J. van Reeuwijk, B. Fischer, A. Rajab, B. Budde, P. Nürnberg, F. Foulquier, D. Lefeber, et al; ARCL Debré-type Study Group. 2008. Impaired glycosylation and cutis laxa caused by mutations in the vesicular H+-ATPase subunit ATP6V0A2. *Nat. Genet.* 40:32–34. doi:10.1038/ng.2007.45

Lee, T., and L. Luo. 1999. Mosaic analysis with a repressible cell marker for studies of gene function in neuronal morphogenesis. *Neuron.* 22:451–461. doi:10.1016/S0896-6273(00)80701-1

Lee, S.H., J. Rho, D. Jeong, J.Y. Sul, T. Kim, N. Kim, J.S. Kang, T. Miyamoto, T. Suda, S.K. Lee, et al. 2006. v-ATPase V0 subunit d2-deficient mice exhibit impaired osteoclast fusion and increased bone formation. *Nat. Med.* 12:1403–1409. doi:10.1038/nm1514

Liégeois, S., A. Benedetto, J.M. Garnier, Y. Schwab, and M. Labouesse. 2006. The V0-ATPase mediates apical secretion of exosomes containing Hedgehog-related proteins in *Caenorhabditis elegans. J. Cell Biol.* 173:949–961. doi:10.1083/jcb.200511072

Lloyd, T.E., R. Atkinson, M.N. Wu, Y. Zhou, G. Pennetta, and H.J. Bellen. 2002. Hrs regulates endosome membrane invagination and tyrosine kinase receptor signaling in *Drosophila. Cell.* 108:261–269. doi:10.1016/S0092-8674(02)00611-6

Lu, H., and D. Bilder. 2005. Endocytic control of epithelial polarity and proliferation in *Drosophila. Nat. Cell Biol.* 7:1232–1239. doi:10.1038/ncb1324

Machen, T.E., M.J. Leigh, C. Taylor, T. Kimura, S. Asano, and H.P. Moore. 2003. pH of TGN and recycling endosomes of H+/K+-ATPase-transfected HEK-293 cells: implications for pH regulation in the secretory pathway. *Am. J. Physiol. Cell Physiol.* 285:C205–C214.

Manolson, M.F., B. Wu, D. Proteau, B.E. Taillon, B.T. Roberts, M.A. Hoyt, and E.W. Jones. 1994. STV1 gene encodes functional homologue of 95-kDa yeast vacuolar H(+)-ATPase subunit Vph1p. *J. Biol. Chem.* 269:14064–14074.

Marshansky, V., and M. Futai. 2008. The V-type H+-ATPase in vesicular trafficking: targeting, regulation and function. *Curr. Opin. Cell Biol.* 20:415–426. doi:10.1016/j.ceb.2008.03.015

Mizushima, N., B. Levine, A.M. Cuervo, and D.J. Klionsky. 2008. Autophagy fights disease through cellular self-digestion. *Nature.* 451:1069–1075. doi:10.1038/nature06639

Morel, N., J.C. Dedieu, and J.M. Philippe. 2003. Specific sorting of the a1 isoform of the V-H+ATPase a subunit to nerve terminals where it associates with both synaptic vesicles and the presynaptic plasma membrane. *J. Cell Sci.* 116:4751–4762. doi:10.1242/jcs.00791

Ng, M., R.D. Roorda, S.Q. Lima, B.V. Zemelman, P. Morcillo, and G. Miesenböck. 2002. Transmission of olfactory information between three populations of neurons in the antennal lobe of the fly. *Neuron.* 36:463–474. doi:10.1016/S0896-6273(02)00975-3

Nishi, T., and M. Forgac. 2002. The vacuolar (H+)-ATPases—nature's most versatile proton pumps. *Nat. Rev. Mol. Cell Biol.* 3:94–103. doi:10.1038/nrm729

Nixon, R.A., D.S. Yang, and J.H. Lee. 2008. Neurodegenerative lysosomal disorders: a continuum from development to late age. *Autophagy.* 4:590–599.

Pelissier, A., J.P. Chauvin, and T. Lecuit. 2003. Trafficking through Rab11 endosomes is required for cellularization during *Drosophila* embryogenesis. *Curr. Biol.* 13:1848–1857. doi:10.1016/j.cub.2003.10.023

Peri, F., and C. Nüsslein-Volhard. 2008. Live imaging of neuronal degradation by microglia reveals a role for v0-ATPase a1 in phagosomal fusion in vivo. *Cell.* 133:916–927. doi:10.1016/j.cell.2008.04.037

Perin, M.S., V.A. Fried, D.K. Stone, X.S. Xie, and T.C. Südhof. 1991. Structure of the 116-kDa polypeptide of the clathrin-coated vesicle/synaptic vesicle proton pump. *J. Biol. Chem.* 266:3877–3881.

Peters, C., M.J. Bayer, S. Bühler, J.S. Andersen, M. Mann, and A. Mayer. 2001. Trans-complex formation by proteolipid channels in the terminal phase of membrane fusion. *Nature.* 409:581–588. doi:10.1038/35054500

Razi, M., E.Y. Chan, and S.A. Tooze. 2009. Early endosomes and endosomal coatomer are required for autophagy. *J. Cell Biol.* 185:305–321. doi:10.1083/jcb.200810098

Rink, J., E. Ghigo, Y. Kalaidzidis, and M. Zerial. 2005. Rab conversion as a mechanism of progression from early to late endosomes. *Cell.* 122:735–749. doi:10.1016/j.cell.2005.06.043

Sann, S., Z. Wang, H. Brown, and Y. Jin. 2009. Roles of endosomal trafficking in neurite outgrowth and guidance. *Trends Cell Biol.* 19:317–324. doi:10.1016/j.tcb.2009.05.001

Südhof, T.C., and J.E. Rothman. 2009. Membrane fusion: grappling with SNARE and SM proteins. *Science.* 323:474–477. doi:10.1126/science.1161748

Sun-Wada, G.H., T. Toyomura, Y. Murata, A. Yamamoto, M. Futai, and Y. Wada. 2006. The a3 isoform of V-ATPase regulates insulin secretion from pancreatic beta-cells. *J. Cell Sci.* 119:4531–4540. doi:10.1242/jcs.03234

Sweeney, S.T., and G.W. Davis. 2002. Unrestricted synaptic growth in spinster-a late endosomal protein implicated in TGF-beta-mediated synaptic growth regulation. *Neuron.* 36:403–416. doi:10.1016/S0896-6273(02)01014-0

Tooze, S.A., and G. Schiavo. 2008. Liaisons dangereuses: autophagy, neuronal survival and neurodegeneration. *Curr. Opin. Neurobiol.* 18:504–515. doi:10.1016/j.conb.2008.09.015

Van Vactor, D.L. Jr., R.L. Cagan, H. Krämer, and S.L. Zipursky. 1991. Induction in the developing compound eye of *Drosophila*: multiple mechanisms restrict R7 induction to a single retinal precursor cell. *Cell.* 67:1145–1155. doi:10.1016/0092-8674(91)90291-6

Wada, Y., G.H. Sun-Wada, H. Tabata, and N. Kawamura. 2008. Vacuolar-type proton ATPase as regulator of membrane dynamics in multicellular organisms. *J. Bioenerg. Biomembr.* 40:53–57. doi:10.1007/s10863-008-9128-z

Wang, T., U. Lao, and B.A. Edgar. 2009. TOR-mediated autophagy regulates cell death in *Drosophila* neurodegenerative disease. *J. Cell Biol.* 186:703–711. doi:10.1083/jcb.200904090

Williamson, W.R., and P.R. Hiesinger. 2010. Preparation of developing and adult *Drosophila* brains and retinae for live imaging. *J. Vis. Exp.* doi:10.3791/1936

Wucherpfennig, T., M. Wilsch-Bräuninger, and M. González-Gaitán. 2003. Role of *Drosophila* Rab5 during endosomal trafficking at the synapse and evoked neurotransmitter release. *J. Cell Biol.* 161:609–624. doi:10.1083/jcb.200211087

Xu, H., S.J. Lee, E. Suzuki, K.D. Dugan, A. Stoddard, H.S. Li, L.A. Chodosh, and C. Montell. 2004. A lysosomal tetraspanin associated with retinal degeneration identified via a genome-wide screen. *EMBO J.* 23:811–822. doi:10.1038/sj.emboj.7600112

Yan, Y., N. Denef, and T. Schüpbach. 2009. The vacuolar proton pump, V-ATPase, is required for notch signaling and endosomal trafficking in *Drosophila*. *Dev. Cell.* 17:387–402. doi:10.1016/j.devcel.2009.07.001

Zhang, J., K.L. Schulze, P.R. Hiesinger, K. Suyama, S. Wang, M. Fish, M. Acar, R.A. Hoskins, H.J. Bellen, and M.P. Scott. 2007. Thirty-one flavors of *Drosophila* rab proteins. *Genetics.* 176:1307–1322. doi:10.1534/genetics.106.066761